The role of grain boundaries in the DC conductivity of *p*-sexiphenyl films

2004 J. Phys.: Condens. Matter 16 2231

(http://iopscience.iop.org/0953-8984/16/13/004)

INSTITUTE OF PHYSICS PUBLISHING JOURNAL OF PHYSICS: CONDENSED MATTER

J. Phys.: Condens. Matter **16** (2004) 2231–2244 PII: S0953-8984(04)74054-0

The role of grain boundaries in the DC conductivity of *p*-sexiphenyl films

S Tkaczyk[1], I V Kityk[1], J Ebothé[2] and R Viennois[3]

[1] Institute of Physics WSP, Aleja Armii Krajowej 13/15, Częstochowa, Poland
[2] Université de Reims, UFR Sciences, LMEN, BP 138, 21 rue Clément Ader, 51685 Reims cedex 02, France
[3] Max-Planck-Institut fur Chemische Physik Fester Stoffe, Nothnitzer Straße 40, D01187, Dresden, Germany

E-mail: i.kityk@wsp.czest.pl

Received 2 January 2004, in final form 17 February 2004
Published 19 March 2004
Online at stacks.iop.org/JPhysCM/16/2231 (DOI: 10.1088/0953-8984/16/13/004)

Abstract

The DC conductivity of *p*-sexiphenyl films 0.2–2.5 μm thick deposited on glass substrates was investigated at temperatures between 4.2 and 300 K to evaluate role of the grain boundary interfaces in the transport properties. Molecular dynamics simulations and quantum chemical modelling of the experimentally observed conductivity have shown that there exist at least three different phases of the films effectively contributing to the observed features of the DC conductivity: conductivity caused by proper crystalline states, conductivity originating from amorphous-like intergrain region and conductivity caused by grain boundaries. A comparison of experimental data with those calculated theoretically shows that the main contribution to the observed DC conductivity is supplied by the boundary region between the crystalline grains and the amorphous-like background, even though this region occupies a relatively low proportion of the total volume.

(Some figures in this article are in colour only in the electronic version)

1. Introduction

Recently, increasing interest in the *p*-sexiphenyl films has been observed. This is caused by their use as materials in light emitting diodes and displays [1, 2]. However, their applications are restricted by the absence of a systematic study of their electronic structure, which prevents efficient design of electronic transport properties to produce a desirable outcome. The existing calculations (even quantum chemical ones) consider this particular material only as amorphous-like, without taking into account the partial ordering in the material [3].

Organic polycrystalline films contain a lot of imperfections that perturb the general distribution of the charge density, which determines the electron transport properties. Such

defect states create a lot of trapping levels within the energy gap, which are energetically more favourable over a wide energy range including the region near the Fermi level. The great abundance of defect states also stimulates the appearance of additional channels for carrier (electron–hole) transport due to the decrease of both the activation barrier energy and the interbarrier work-function. This suggests that a suitable variation of structural parameters can change the electronic parameters in a desired direction. The coexistence of different states leads to the occurrence of different physical mechanisms that determine the corresponding transport properties, most importantly the conductivity. A deviation from the classical transport of thermally activated carriers observed in disordered materials provided the background of the hopping model with a range of variable conductivity features [4, 5]. For a deeper understanding of electrical properties, we should consider the charge transport, particularly that due to the carrier diffusion and specific current flow.

The main goal of the present work consists in the study of the role played by the grain boundaries in the electronic transport properties of *p*-sexiphenyl films, particularly in the DC conductivity. We proceed to experimental measurements on the films using different electrode polarities, film thicknesses and temperatures. Simultaneously, theoretical molecular dynamics and quantum chemical simulations are executed. A comparison of experimental results with the results of the simulations performed is crucial for evaluating the contribution of each of the different parts of the films in the output DC conductivity.

2. Technology of sample preparation

As raw materials for the film deposition, *p*-sexiphenyl powder with chemical purity 99% *m*-terphenyl (1,3-diphenylobenzene) produced by Tokyo Kasei Co. Ltd, having stoichiometry $C_{36}H_{26}$ with molecular mass equal to 458.59, was used. The sexiphenyl films were deposited by sublimation in vacuum (at a pressure of about 6.5×10^{-6} Torr). Glass BK7 was used as a substrate, on which gold electrodes were evaporated. Under the same vacuum sublimation conditions, the appropriate *p*-sexiphenyl layers were deposited, followed by evaporated Al layers on the surfaces. These Al layers form the second electrodes. The evaporated film thickness was varied from 0.2 up to the 2.5 μm and the non-homogeneity did not exceed 0.2%. The thickness of the metal electrodes was varied within the range 0.2–0.4 μm. The DC conductivity between the gold and aluminium electrodes and vice versa was measured for different electrode polarities. The general geometry of the electrodes is shown in figure 1.

We have found that during sublimation under vacuum the radially oriented MC morphology appears. The microcrystallite (MC) sizes were evaluated using optical polarized microscopy. The morphology of the MC shows the appearance of slightly agglomerated spherolites.

The MC sizes and their orientation are dependent on the film thickness. In fact, one observed that increase of the film thickness leads to increase of the MC size.

The measurements of the DC conductivity were conducted using a DC current flowing through the sample between the gold and aluminium electrodes. The current was measured using an electrometer, CARY 401 (vibration condensator), within 1.2×10^{-18}–3.2×10^{-8} A and the Advantest R8240 for the current range 10 fA–20 mA. These electrometers were connected to the IEEE 488 electronic interface which allows about 75 measurements per second. The distance between the electrodes (corresponding to the film thickness) varies within 0.2–2.5 μm. The film thickness was monitored independently using a standard interferometric optical method.

The measurements were performed for different (Au–Al) electrode polarizations in the voltage range 0–200 V, varying the temperature between 20 and 325 K.

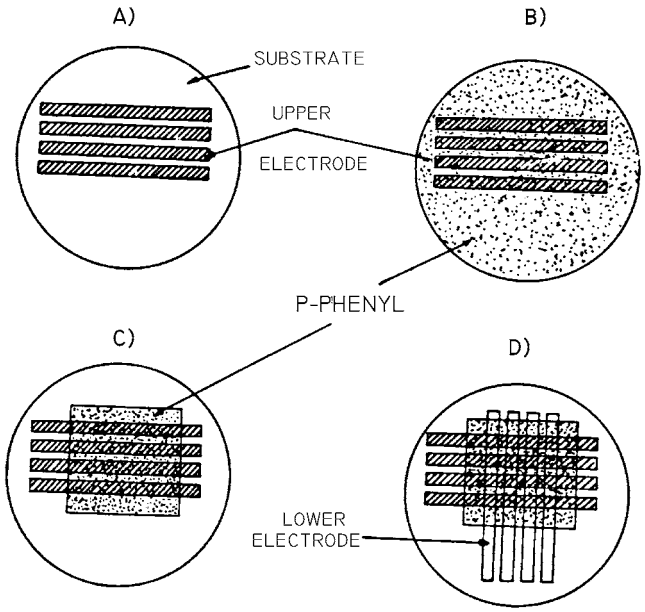

Figure 1. The general geometry of the electrodes and substrates. The diameters of the glasses was about 40 mm. The widths of the electrodes (upper gold and lower aluminium) were 2 mm; *p*-sexiphenyl surface: 20 mm × 20 mm.

The carrier mobility was monitored by conventional time of flight (TOF) techniques. The measurements were done at room temperature. A nitrogen UV laser (at wavelength 337 nm; 1 ns pulse duration) was used for the photogeneration of free carriers. The experiment was done at small signal in the TOF method, the transient current being measured with a digital oscilloscope. The drift mobility was determined from the expression $\mu = \frac{x}{Ft_{\mathrm{T}}}$, where F is the applied field; x, the efficient film thickness for the charge transfer, was determined from the intersection of the asymptotes and the trailing edge of the transient. The time where this occurs is that of the arrival of the carrier front sheet at the opposite electrode.

3. Experimental results

Typical DC I (current)–V (voltage) experimental results for the *p*-sexiphenyl films are shown in figure 2. Additionally, we present the corresponding $\ln(I) = f(1/k_{\mathrm{B}}T)$ curves (see figures 3 and 4) from which are determined, at the positive sign linear parts of the curve, the two main parameters, $E1$ and $E2$, known as the activation energies. The quantum chemical simulations performed within the quantum chemical semi-empirical AM1 methods have shown that $E1$ prevailingly originates from the film's proper conductivity while $E2$ corresponds to conductivity mainly due to the interface trapping levels. From figures 3 and 4, one can also see regions possessing a slight dependence of $\ln(I)$ versus temperature. This may indicate a hopping (non-activating) type of conductivity which will be a subject of future work. In figure 3, one can see a significant current decrease of about 100 K, which may reflect typical activation energy hopping.

Independently performed measurements, using TOF experiments, have shown that the observed conductivity has a hole origin. The maximal mobility achieved was equal to about 1.3×10^{-2} cm^2 V^{-1} s^{-1}. So the role of the hole in the transport properties of *p*-sexiphenyl

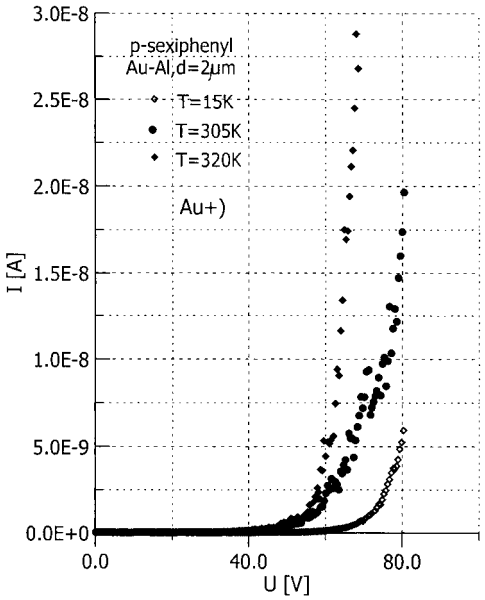

Figure 2. A typical $I = f(U)$ dependence for the p-sexiphenyl films.

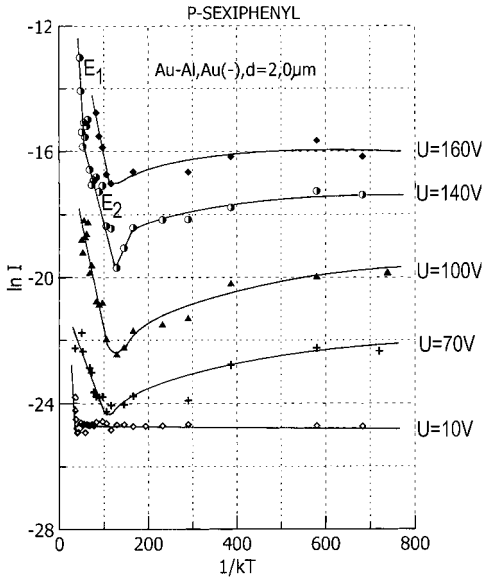

Figure 3. The dependence $\ln I = f(kT^{-1})$ for p-sexiphenyl films; Au–Al, for different voltage electrode polarities, sample thickness $d = 2.0$ μm.

should be predominant. Assuming that the transport mechanisms are prevailingly originating from the holes in p-sexiphenyl, we have calculated the activation energy parameters, which are presented in table 1. For example, our evaluation has shown that for the Au–Al electrodes at 2.0 μm film thickness, $E_{\mathrm{T}} = 0.000\,43$ eV at $T = 5$ K and 0.280 eV at 325 K. The reported parameters are evaluated for samples of different thicknesses and at different temperatures.

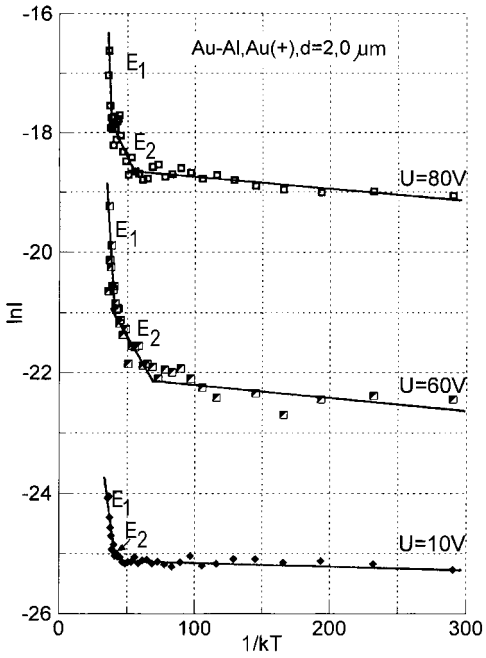

Figure 4. The dependence $\ln I = f(kT^{-1})$ for *p*-sexiphenyl films; Au–Al, for different voltage electrode polarities, sample thickness $d = 2.0$ μm, electrode polarity Au(+).

Table 1. . Activation energies $E1$ and $E2$ at different voltages and for the film thickness 2.0 μm. The precision of the energy determination is about 0.0001 eV.

		Au(+)		Au(−)	
N	*U* (V)	*E*1 (eV)	*E*2 (eV)	*E*1 (eV)	*E*2 (eV)
1	5	0.16	0.003	0.250	—
2	10	0.16	0.001	0.260	—
3	15	0.20	0.002	0.320	
4		0.244	0.002	0.290	
5	25	0.244	0.003	—	
6	30	0.241	0.002		
7	35	0.133	0.001	—	
8	40	0.279	0.002	0.500	
9	45	0.232	0.004	—	
10	50	0.266	0.007	0.800	
11	55	0.169	0.007	—	
12	60	0.169	0.005	0.600	—
13	65	0.198	0.005	—	—
14	70	0.194	0.005	0.570	0.070
15	75	—	0.004	—	—
16	80	0.139	0.005	0.200	0.045

The changes in electrode polarities do not sensitively affect the conductivity (see figure 5) at relatively high temperatures (higher than 55 K). However, at low temperatures (compare figures 6–8), and particularly for the thickness values below 1.5 μm, one can see that the observed differences are noticeable. The potential barriers for Au and Al are equal to 5.2 and

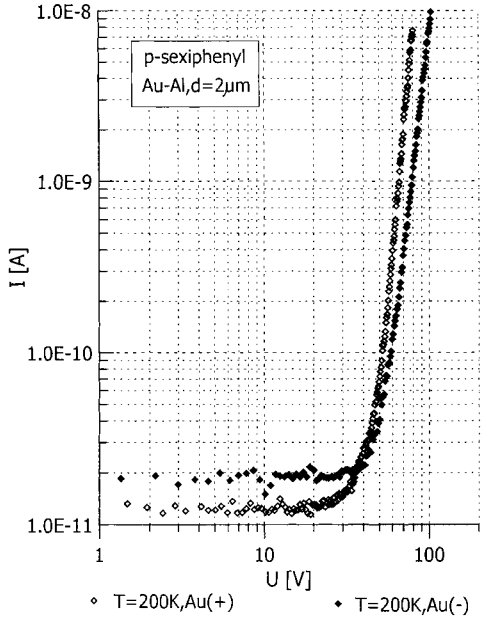

Figure 5. The dependence of $I = f(U)$ (log plot) for p-sexiphenyl for temperature $T = 200$ K; Au–Al, Al(−).

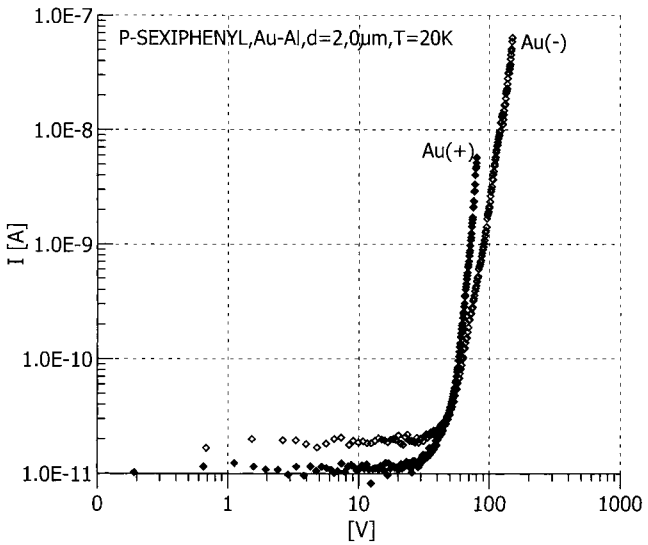

Figure 6. Current–voltage characteristics for polycrystalline films made up of p-sexiphenyl layers. The dependence $I = f(U)$ (log plot) for temperature $T = 20$ K; Au–Al, $d = 2\,\mu$m, using different polarities of electrodes.

4.3 eV, respectively. From the experimental current–voltage (I–V) curves, we have determined the DC conductivity activation energy for various applied voltages.

For an appropriate description of the observed dependences we have included the activation work-function $E_{\mathrm{a}}^{(\mathrm{eff})}$ in the case of prevailingly hole carriers that was evaluated by means of

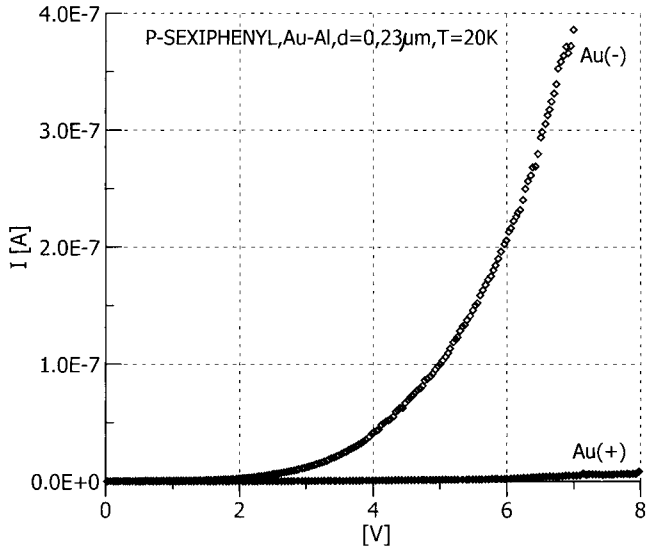

Figure 7. Current–voltage characteristics for polycrystalline films made up of *p*-sexiphenyl layers. The dependence $I = f(U)$ (log plot) for temperature $T = 20$ K; Au–Al, $d = 0.23$ μm, using different polarities of electrodes.

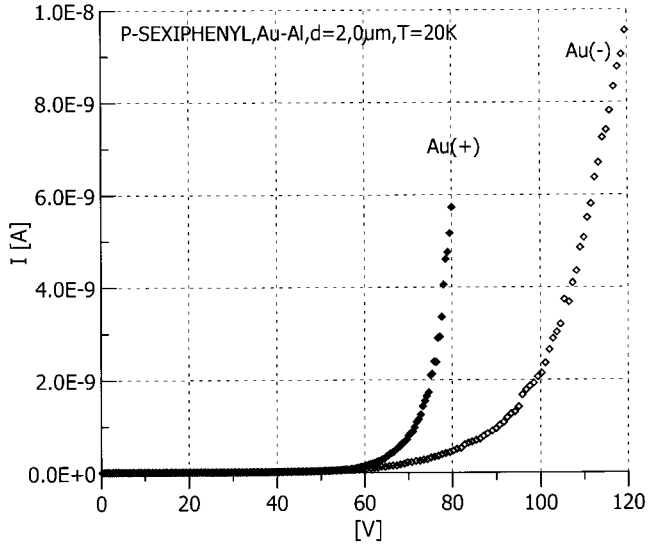

Figure 8. Current–voltage characteristics for polycrystalline films made up of *p*-sexiphenyl layers. The dependence $I = f(U)$ (log plot) for temperature $T = 20$ K; Au–Al, $d = 2$ μm, using different polarities of electrodes.

expression [16]:

$$E_{\mathrm{a}}^{(\mathrm{eff})} = \frac{1}{\bar{E}_{\mathrm{c}}} \int_0^x \mathrm{d}l \int_0^{\bar{E}_{\mathrm{c}}} g \bullet \exp\left(-\frac{(E_a^{(g)} - E)}{kT}\right) \mathrm{d}E \tag{1}$$

where: $E_{\mathrm{a}}^{(g)}$ is the activation energy determined from the experimental $\ln(I) = f(1/kT)$ curve for a given thickness value x (see figures 3 and 4); $\bar{E}_{\mathrm{c}}$ is the range of energy changes; g is

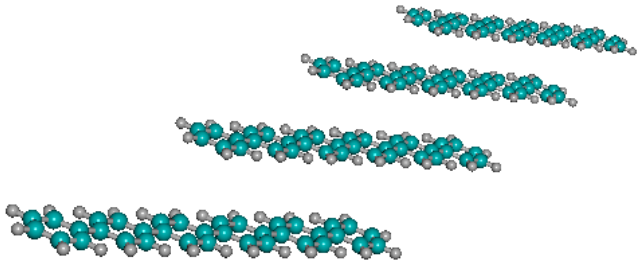

Figure 9. The layer-like structure of the sexiphenyl crystallites.

the degeneracy of the particular energy term; x is the film thickness. Using the measurements performed for films of different thicknesses, at different temperatures and external electric fields (see figures 6–8), we have obtained a set of equations containing $E_a^{(\mathrm{eff})}$, film thickness D etc. At the same time we have verified, using Monte Carlo simulation, the dependence of the different parameters on the charge carrier transport which was described by equation [17]:

$$\mu = \mu_0 \exp\left(-(3\sigma/5kT)^2 + C_0\left((\sigma/kT)^{3/2} - \Gamma\right)\sqrt{\frac{eRF}{\sigma}}\right), \tag{1a}$$

where: $C_0 = 0.89$ and $\Gamma = 1.82$ are pre-exponential factors; R is the distance between transport sites; σ is the root mean square width of the dipolar energy disorder. A key parameter of the model was determined by the dipoles existing in the system and it has a relation to the parameter $\sigma = 2.35ep/(er^2)$, where: p is the state dipole moment of the molecule; r is the interdipole distance; ε is the dielectric constant of the medium.

The calculations of the current I in the model described by (1) and (1a) have shown an agreement up to 4.6%, which may indicate a correct feature of the adopted model.

To provide physical insight into such behaviour, we present the main calculated energy level diagram, in figure 12. The related $E_a^{(\mathrm{eff})}$ values obtained correspond to the energy of the maximal trapping density of states calculated assuming that the activated charge transport prevails, the polaron binding energy being negligible. This could be justified by the high value of the activated energy [18].

Substantial thickness differences obtained for the films investigated (figure 9) should indicate a substantial contribution of the intergrain regions for MC sizes comparable to the film thickness.

The effective conductivity is evaluated using the expression

$$\sigma \cong \exp\left(-\frac{|E_a^{(\mathrm{eff})} - eU/Dx|}{kT}\right), \tag{2}$$

where: U is the applied voltage; T is the actual temperature; D is a coefficient related to the renormalization of the external voltage due to the carrier diffusion; x is the effective length of film determined from the following expression:

$$N(t) \cong N_0 \exp\left(-\frac{x^2}{Dt}\right), \tag{3}$$

where: x is the thickness of the p-sexiphenyl film; t is the time for the diffusion process considered determined by the corresponding work-function; N_0 is the carrier concentration at the beginning of the diffusion process considered; E_a^{eff} is the effective activation energy averaged from those of the crystalline part, the amorphous part, the trapping levels of the grain boundary and the Fermi levels of the metal electrode.

4. Molecular dynamics simulations of the microcrystallite subsystem

For the description of the particular long range ordered microcrystallites, we performed a calculation of the total band energy for a crystalline structure (space group $P2_1a$) and amorphous-like (disordered) phases of *p*-sexiphenyl.

4.1. Amorphous molecule

The total energy was calculated using the norm-conserving pseudopotential scheme reported in [6]. The molecular mechanics (MM) method is promising and suitable for treating the properties of large molecular systems. Recently, it has been extensively used in biochemical simulations. However, there are significant limitations as regards its application, commonly due to the classical feature of the MM: force fields [19]. As an example, the use of MM schemes for treating chemical reactions, including the formation of bonds and transition states, and for treating highly correlated compounds such as rare earth clusters is impossible or, at least, questionable since the main requirement for application of this scheme is the existence of a ground electronic state in the molecule involved, without low lying singly excited CI states. Moreover, the MM approaches generally need sophisticated parametrization for the fitting procedure. The main advantage of the MM schemes is their lower expense and good reliability in the prediction of molecular structure for organic compounds having a weak electron correlation. At the same time, the main advantage of the QM (quantum mechanical) procedures is the wide range of problems they may solve. It could be imagined that an appropriate QM description in the MM framework would give substantially better results. This approach, which is an alternative to the construction of QM schemes with $O(N)$ scalability, appears to create quantum mechanical/molecular mechanical (QM/MM) schemes, providing another way to overcome the drawback of N^n scalability. The QM/MM approaches are suitable for treating a relatively low proportion of the observed chemical transformations. At the same time, many systems can be considered within the classical approach. The benefit of the application of these methods is that they can follow chemical transformations which usually affect only a small part of the whole system—in particular, those for a molecule embedded in an amorphous-like background. This is the case here, for our partially crystallized films.

The calculations have been basically done here following the procedure of [20] which is acquiring increasing popularity. This procedure includes hybrid QM/MM schemes suitable for treating large molecular systems. It is here additionally modified by the different approaches reported in [21, 22]. For a strict comparison of the results, we have done calculations using the polarizable continuum model described in the [23]. It was found that the convergence of the method for the sexiphenyl investigated is slow and the stability of the complexes not better than that found in the QM/MM approach described.

The approach described briefly above was verified by us earlier for other partially ordered solid state systems. For the details see [24–26].

4.2. Crystalline and quasi-crystalline approaches

While doing the calculations for the crystalline and partially crystalline materials we have also done calculations using the structure factors of structurally perfect crystalline *p*-sexiphenyl. The pseudopotential was represented in a Gaussian–polynomial form. Following the optimized grain geometry, we have included an additional structural disordering parameter, which is responsible for the disappearance of the crystalline long range ordering. This parameter is particularly important for the interfaces separating the MC and the amorphous-like background.

Assuming a sphere-like shape for the MC and an equilibrium deposition process, one can expect the growing MC sizes to be limited by the interface potential gradients arising.

A similar superposition of the different structural fragments has been successfully used for solid binary alloys [7], glasses and organic materials [8]. Therefore, this approach is expected to be sufficient for different disordered materials and partially ordered solids such as the MC investigated here. We select a plane-wave basis set formed by 324–564 plane waves to achieve eigenenergy convergence of about 0.012 eV.

The solution of the secular equation set was obtained using a modified Jacobi method QL. Additional (676–928) plane waves from an extended Lowdin basis set were included in the calculations. Electron screening effects were taken into account using a parametrized Perdew–Zunger expression [9]. The special Chadi–Cohen point method [10] was applied in the calculation of the spatial distribution of the electron charge density. A diagonalization procedure was carried out at special weighting points of the BZ for each MC type.

Acceleration of the iteration convergence was achieved by transferring 75% of the $(m-1)$th iteration result to the mth iteration. We assumed a level of calculation error (ε) better than 0.10%.

To study how the results of the band structure calculations depend on the choice of the MC, additional calculations for perfect n-phenyl crystalline phases ($P2_1a$) were done. A coincidence of the eigenenergies within 3.2% was achieved. The main drawback of all one-electron calculations consists in an underestimation of the band energy gap values. For this reason, a self-energy correction renormalization procedure was included in the energy gap calculations.

The electron structure of the amorphous-like background was calculated using quantum chemical simulations following the method described in [11–14]. As geometric cluster boundary parameters, we used the first and second coordination spheres for the sexiphenyl background. Using the same approach, the BK7 glass substrate contributions were considered.

The effective total potential was built as a superposition of amorphous-like long range background (intergrain regions) and local MC contributions.

In addition, a total energy minimization of the clusters was performed using the space derivative of the potentials on the borders between the particular phases. The total energy of the MC film was evaluated as a statistical sum renormalized by an appropriate Boltzmann weighting factor [11].

The geometry optimization was performed using the molecular dynamics technique described in [15]. Several approaches taken from Becke's scheme [15] involving a semi-empirical contribution to the 'exact' exchange were also applied.

In the case of the amorphous-like disordered system, we applied a variational procedure following a Green function formalism [16–19].

The geometry optimization procedure was started from the interfaces between the MC boundary, the amorphous-like phase and the glass background. Afterwards, we successively applied a similar procedure for the next layer. The iteration began from the bulk MC region and subsequently penetrated into the disordered amorphous-like region. We started from the molecular dynamics interface optimization of the four neighbouring layers (two from the MC side and two in the direction of the amorphous-like background). About 70–120 atoms from both sides of the interface were considered. The molecular dynamics procedure was continued until the total minimum energy value for a given cluster was the same as that for the whole compound. The step-by-step procedure was repeated through an iteration process until the relative displacement of atoms for two successive layers was less than 0.24 Å.

To achieve sufficient molecular dynamics geometry convergence, it was necessary to take into account from 8 to 12 such layers.

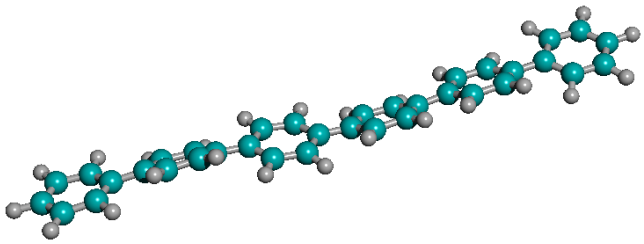

Figure 10. Non-planarity of the starting molecule.

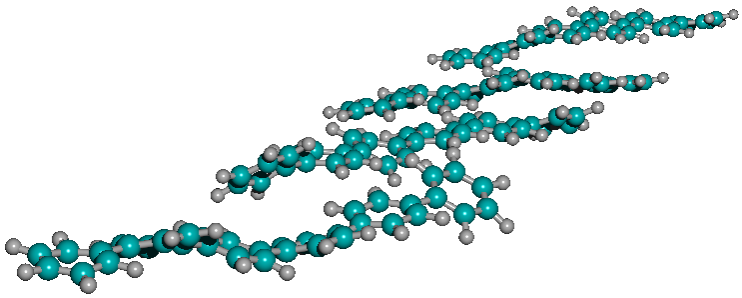

Figure 11. The grain boundary topology of the sexiphenyl films.

5. Results and discussion

The MD simulations performed have shown that there exist at least three different phases in the sexiphenyl films investigated, contributing differently to the DC conductivity. We have demonstrated that the layer-like packing (see figure 9) during the approach to the MC boundaries becomes markedly non-planar (see figure 10). During the performance of the molecular structure optimization, the interface considered obtains a very sophisticated surface topology (see figure 11). The TEM microscopic data together with the appropriate molecular dynamics simulations have shown that the amorphous-like background covers almost 79% of the film volume: the polycrystalline phase takes up about 16% while the MC grain boundary region is only 5%. As a proof of the chosen theoretical approach, one can cite the good agreement between the changes of the structural data obtained experimentally and from simulations. This agreement was within 6%.

However, the trapping levels created by the grain boundaries hit within the forbidden energy gap (see figure 12), where the occurrence of transport activation processes is expected. These levels in the DC conductivity should be sufficiently higher than the electronic bands formed by the crystalline and amorphous-like parts of the films. Simultaneously, the large potential gradients on the boundary may stimulate a dipole moment increase which is directly related to the hole mobility and conductivity. As a consequence, the contribution of the corresponding levels in the total conductivity should be crucial (see figure 13).

The great role played by the boundaries may be used during future synthesis of *N*-phenyl films. The experimental data presented unambiguously show that a variation of the film thickness within 2–10 μm leads to a variation of the grain size along with the boundary surfaces. Moreover, appropriately varying the type of electrode, and the corresponding potential barriers, the boundary size corresponding to the maximal conductivity could be achieved.

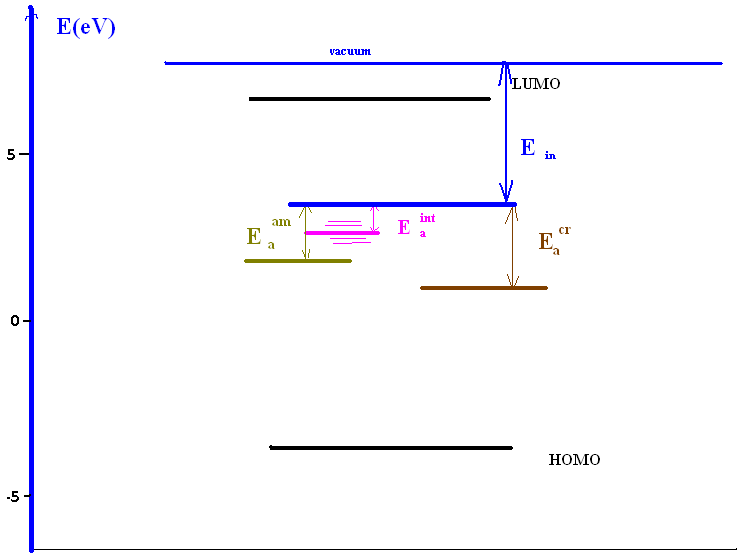

Figure 12. The principal energy diagram for the levels in the sexiphenyl films.

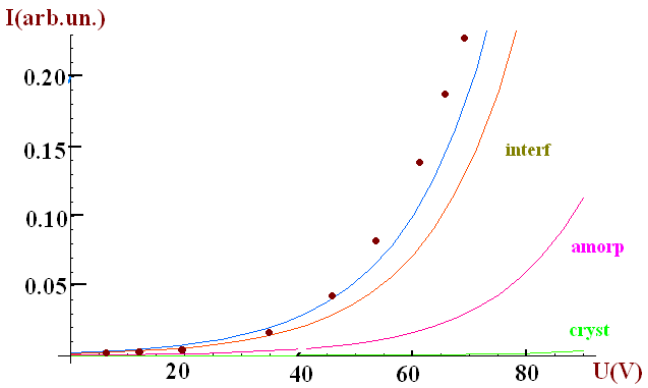

Figure 13. Simulated behaviour of the $I = f(U)$ dependence of the p-sexiphenyl films originating from the contributions of different parts. Experimental data are shown by points. Their parameters were obtained from the MD simulations, as described in the text.

The layered MC structure dictates a strong anisotropy for particular crystallites. When nearing the MC borders, the benzene rings become non-planar within a particular molecule (see figure 10). This might be important for the determination of the optimal MC size. In the amorphous-like phase, the torsion angles (evaluated from the MD simulations) between the benzene planes vary within 20°–46° (for comparison, the experimental data give corresponding values of about 25°–42°). The electronic properties, for this case, should be more isotropic as compared to those of the perfect crystals and the grain boundary regions should become more interesting as regards electron transport properties (see figure 11). In addition to intraplanar ordered bonds, interlayer bonds occur which may form further new topology features for the carrier transport—particularly those for the intermediate types lying between the two- and three-dimensional configurations with large interborder potentials. The interface potential jumps lead to very large local potential space gradients forming large dipole moments as well

as a large number of trapping levels. The experimental data (see figures 3 and 4) clearly show the existence of two main activation mechanisms. The first one (indicated by $E1$) is created by appropriate carrier transport properties and the second one ($E2$) is governed by the above mentioned grain boundary trapping levels. The role of the other mechanisms, particularly the hopping, is not yet clarified and hence requires additional investigation. This is supported also by the changes of electrode polarities at different temperatures.

Using the existing structural and quantum chemical data, we were able to calculate the main energy parameters presented in figure 12. We have found that the averaged activation energy for a crystalline phase is $E_a^{cr} \approx 0.27$ eV; for the amorphous-like structure the corresponding parameter is $E_a^{am} \approx 0.21$ eV while grain boundaries lead to $E_a^{int} \approx 0.08$ eV. The values obtained for the activation energies are at least 12% lower than similar values presented in the figure 8 of [16], where terphenyl and quaterphenyl films were investigated. This reflects the substantially lower effective energy gap in the sexiphenyl films investigated as compared with the terphenyl and quaterphenyl films.

All the parameters were evaluated with respect to the metallic Fermi energy E_F. The calculated $I = f(U)$ dependences originating from the different parts of the film are very close to the experimental one (see figure 13), which shows a good agreement between the proposed theoretical approach and the observed experimental data. The simulations performed show that for an appropriate variation of the grain size and film thickness there is a possibility for further enhancement of the DC conductivity.

A comparison of the different contributions to the DC conductivity obtained from the method described above has shown (figure 13) that the grain boundaries supply the main contribution to the observed susceptibility. However, this susceptibility can also vary because of particular contributions from the amorphous-like and crystalline phases. This finding seems to be very important from the applications point of view because the above mentioned structures are widely used in different optoelectronic devices (LED, displays etc); the main complication that restricts their larger application consists in a degradation of the transport properties. A knowledge of the grain boundary properties, which are sensibly more stable than those of the amorphous-like phase, provides here a possibility for stabilizing their parameters during their exploitation. In particular, it will be very important to study the role of electron–phonon trapping, which is tremendously sensitive to temperature.

The results obtained show that the widely adopted approach that considers sexiphenyl films as homogeneous amorphous-like media is not sufficient when searching for new more efficient carrier transport. A good agreement of the calculations performed with the experimental data indicates the efficacy of the present approach in describing the observed transport properties, particularly the DC conductivity. A variation of the film structure can lead to a variation of its optoelectronic properties in a desirable direction.

6. Conclusions

A crucial role of the microcrystalline grain boundaries in the observed transport properties of sexiphenyl films was demonstrated. To describe the carrier kinetics in sexiphenyl films, a complex approach including molecular dynamics grain boundary structure optimization, band structure calculations and experimental DC conductivity measurements versus temperature, film thickness and electrode polarity were applied. The contribution to the observed DC conductivity of the microcrystalline grain boundaries prevails even though their contribution to the film's volume does not exceed 5%. The widely adopted approach of considering sexiphenyl films as homogeneous media is not sufficient when searching for enhanced transport properties. Only an appropriate modification of the films, particularly of their MC structure,

may change the corresponding DC parameters in the desirable direction. The experimental data presented concerning the thickness dependence at different temperatures confirm that only actual variation of the film thickness and the related grain sizes is a feasible approach for improving the transport properties.

References

[1] Ohmori Y, Tsukagawa T and Kajii H 2001 *Displays* **22** 427
[2] Yanagi H, Okamoto S and Mikami T 1997 *Synth. Met.* **91** 91
[3] Koch N, Parente L-M, Lazzaroi L, Johnson R L, Leising G, Pireaux J-J and Bredas J-L 1999 *Synth. Met.* **101** 438
[4] Mott N F 1971 *Phil. Mag.* **24** 91
[5] Voegle V, Kalbitzer H and Boringer K 1985 *Phil. Mag.* B **52** 153
[6] Bachelet G B, Hamann D R and Schluter M 1982 *Phys. Rev.* B **26** 4199
[7] Kityk I V, Fahmi A, Sahraoui B, Rivoire G and Feeks I 2001 *Opt. Mater.* **16** 417
[8] Kityk I V, Sahraoui B, Nguyen P X, Rivoire G and Kasperczyk J 1997 *Nonlinear Opt.* **18** 13
[9] Perdew J B and Zunger A 1981 *Phys. Rev.* B **23** 5048
[10] Chadi D J and Cohen M L 1973 *Phys. Rev.* B **8** 5747
[11] Czerwinski M, Mervinskii R I, Kulesza M, Kityk I V and Kasperczyk J 1998 *Mater. Chem. Phys.* **56** 7
[12] Kityk I V 2001 *Opt. Laser Eng.* **35** 239
[13] Kityk I V, Kasperczyk J and Andrievskii B V 1996 *Phys. Lett.* A **216** 16
[14] Kityk I V and Sahraoui B 1999 *Phys. Rev.* B **60** 942
[15] Becke A D 1994 *J. Chem. Phys.* **67** 2567
[16] Tkaczyk S, Kityk I V and Schiffer R 2002 *J. Phys. D: Appl. Phys.* **35** 563
[17] Novikov S V, Dunlap D H, Kenkre V M, Parris P E and Vannikov A V 1998 *Phys. Rev. Lett.* **81** 4472
[18] Schein L B, Glatz D and Scott J C 1990 *Phys. Rev. Lett.* **65** 472
[19] Tchougréeff A L 1997 *Khim. Fiz.* **16** 62
Tchougréeff A L 1997 *Chem. Phys. Rep.* **16** 1035 (Engl. Transl.)
[20] Warshel A and Levitt M 1976 *J. Mol. Biol.* **103** 227
[21] French S A, Sokol A A, Bromley S T, Catlow C R A, Rogers S C, King F and Sherwood P 2001 *Angew. Chem.* **113** 4569
[22] Tokmachev A M, Tchougréeff A L and Misurkin I A 2000 *THEOCHEM* **506** 17
[23] Barone V, Cossi M and Tomasi J 1998 *J. Comput. Chem.* **19** 404
[24] Sahraoui B, Kityk I V, Phu X, Hudhomme P and Gorgues A 1999 *Phys. Rev.* B **59** 9229
[25] Kityk I V 2003 *Semicond. Sci. Technol.* **18** 1001
[26] Kityk I V 2003 *Comput. Mater. Sci.* **27** 342